

CRACK DETECTION BY SPATIO-TEMPORAL GRADIENT ANALYSIS OF THE ACOUSTIC SURFACE WAVE FIELD

PACS REFERENCE: 43.35.Zc

Teramoto, Kenbu
Department of Mechanical Engineering, Saga University
1- Honjo, Saga-shi, SAGA,
8408502, JAPAN
Tel: +81-952-28-8622
FAX: +81-952-28-8587
E-mail: tera@me.saga-u.ac.jp

ABSTRACT

This paper presents a crack characterization method by spatio-temporal gradient analysis over the surface elastic wave field. The surface ultrasound wave that propagates in the direction of the layer is a potential candidate of non-destructive evaluation. The proposed method has an ability to classify the surface acoustic wave field through the rank of the covariance matrix defined over the 4-dimensional vector space which is spanned by following components: a vertical displacement, its vertical velocity, and a pair of shear strains. The determinant of the covariance matrix, therefore, is proposed as the index of homogeneity of the object surface.

INTRODUCTION

Lamb waves play important roles in NDE fields. A point source placed on the surface of a homogeneous isotropic plate excites several kinds of waves: (a) pressure and shear waves propagating in the medium, (b) a Rayleigh wave that is confined to the surface of the medium, and (c) symmetric and anti-symmetric Lamb waves traveling along the plate. The first two waves are utilized for traditional ultrasonic techniques such as pulse-echo methods. In contrast to these classical techniques, in which the wavelengths are shorter than the plate thickness, the Lamb waves have the advantage of propagating over large area, thus interrogating the entire specimen, including inaccessible portion of the objects. Unfortunately, the velocity of each mode of Lamb waves varies with frequency. Consequently the detected ultrasound signals are very complicated, causing difficulties in signal interpretation. It is important, therefore, to establish the signal detection criterion independent of local wave numbers. In this paper, the theoretical derivation of the index of homogeneity based on the spatio-temporal gradient analysis is described. Next, the governing equations are briefly outlined. In the third section, several numerical experiments evaluate the proposed index that visualizes the existence of cracks on the object surface. Finally, the advantages of the proposed index of homogeneity is discussed and evaluated.

PROBLEM FORMULATION

Wave Fields on Non-Absorbing Plate In Vacuum

Considering single sound source at the origin on the plate of thickness $2h$, density ρ , longitudinal velocity C_L , and shear velocity C_T , the general displacements normal to the plate are given by the combination of the following symmetric and anti-symmetric forms:

$$u_{sz}(\mathbf{r}, t) = \frac{1}{\sqrt{\|\mathbf{r}\|}} (a_{zL} (\exp(-j\beta_L h)) - \exp(j\beta_L h)) + a_{zT} (\exp(-j\beta_T h) - \exp(j\beta_T h)) \exp(j(\omega t - \mathbf{k}^T \mathbf{r})), \quad (1)$$

$$u_{az}(\mathbf{r}, t) = \frac{1}{\sqrt{\|\mathbf{r}\|}} (a_{zL} (\exp(-j\beta_L h)) + \exp(j\beta_L h)) + a_{zT} (\exp(-j\beta_T h) + \exp(j\beta_T h)) \exp(j(\omega t - \mathbf{k}^T \mathbf{r})), \quad (2)$$

where ω is the circular frequency, \mathbf{k} is the wave number vector and \mathbf{r} is the coordinate on the surface of the plate. The wave numbers for the normal direction, satisfy the following relations:

$$\beta_L = \sqrt{\left(\frac{\omega}{C_L}\right)^2 - \|\mathbf{k}\|^2}, \quad \beta_T = \sqrt{\left(\frac{\omega}{C_T}\right)^2 - \|\mathbf{k}\|^2}. \quad (3)$$

Solving the above equations of motion under the stress free surface boundary conditions, the symmetric and anti-symmetric of Lamb waves satisfy the following dispersion equations respectively:

$$\frac{\tan(\beta_T h)}{\tan(\beta_L h)} = -\frac{4\beta_L \beta_T \|\mathbf{k}\|^2}{(\|\mathbf{k}\|^2 - \beta_T^2)^2}, \quad \frac{\tan(\beta_L h)}{\tan(\beta_T h)} = -\frac{4\beta_L \beta_T \|\mathbf{k}\|^2}{(\|\mathbf{k}\|^2 - \beta_L^2)^2}. \quad (4)$$

Description of Spatio-temporal Gradient Field

Let the normal displacement, $f(x, t)$, be denoted by the sum of a symmetric wave $u_{sz}(\mathbf{r}, t)$ and an anti-symmetric wave $u_{az}(\mathbf{r}, t)$ as:

$$\begin{aligned} f(\mathbf{r}, t) &= u_{sz}(\mathbf{r}, t) + u_{az}(\mathbf{r}, t) \\ &= \frac{1}{\sqrt{\|\mathbf{r}\|}} ((a_{zL} (\exp(-j\beta_L h)) - \exp(j\beta_L h)) \\ &\quad + a_{zT} (\exp(-j\beta_T h) - \exp(j\beta_T h)) \\ &\quad + a_{zL} (\exp(-j\beta_L h)) + \exp(j\beta_L h)) \\ &\quad + a_{zT} (\exp(-j\beta_T h) + \exp(j\beta_T h)) \exp(j(\omega t - \mathbf{k}^T \mathbf{r})). \end{aligned} \quad (5)$$

Consequently, the temporal and spatial derivatives at the point \mathbf{r} can be denoted as follows:

$$\begin{aligned} f_t(\mathbf{r}, t) &\triangleq \frac{\partial f(\mathbf{r}, t)}{\partial t} = j\omega f(\mathbf{r}, t), \\ f_x(\mathbf{r}, t) &\triangleq \frac{\partial f(\mathbf{r}, t)}{\partial x} = \xi_x f(\mathbf{r}, t) + \tau_x f_t(\mathbf{r}, t), \\ f_y(\mathbf{r}, t) &\triangleq \frac{\partial f(\mathbf{r}, t)}{\partial y} = \xi_y f(\mathbf{r}, t) + \tau_y f_t(\mathbf{r}, t). \end{aligned} \quad (6)$$

Here the four coefficients, ξ_x , ξ_y , τ_x , and τ_y are respectively given by:

$$\xi_x = -\frac{\mathbf{r}^T \mathbf{e}_x}{2\|\mathbf{r}\|^2}, \quad \xi_y = -\frac{\mathbf{r}^T \mathbf{e}_y}{2\|\mathbf{r}\|^2}, \quad \tau_x = -\frac{\mathbf{k}^T \mathbf{r} \mathbf{r}^T \mathbf{e}_x}{\omega \|\mathbf{r}\|^2}, \quad \tau_y = -\frac{\mathbf{k}^T \mathbf{r} \mathbf{r}^T \mathbf{e}_y}{\omega \|\mathbf{r}\|^2}. \quad (7)$$

It is clear from the above equations that the normal displacement and the particle velocity are linearly dependent on the corresponding spatial derivatives when unique sound source exists on the plate.

Index of Homogeneity

For determination of the linear dependency among the above four time varying signals, a short duration ($=t_0$) correlation matrix is introduced as follows:

$$\Phi = \int_0^{t_0} \mathbf{f} \mathbf{f}^T dt = \begin{pmatrix} \phi_{xx} & \phi_{xy} & \phi_{xt} & \phi_x \\ \phi_{yz} & \phi_{yy} & \phi_{yt} & \phi_y \\ \phi_{tz} & \phi_{ty} & \phi_{tt} & \phi_t \\ \phi_x & \phi_y & \phi_t & \phi \end{pmatrix} = \begin{pmatrix} \Phi_{11} & \Phi_{12} \\ \Phi_{12} & \Phi_{22} \end{pmatrix}, \quad (8)$$

where, the time varying four dimensional vector \mathbf{f} is denoted as:

$$\mathbf{f} = (f_x(\mathbf{r}, t) \quad f_y(\mathbf{r}, t) \quad f_t(\mathbf{r}, t) \quad f(\mathbf{r}, t))^T. \quad (9)$$

When no crack exists on the plate surface, unique sound source causes the linear dependency between two vectors, among four components. Thereupon, the following equation is satisfied:

$$\det(\Phi_{11})\det(\Phi_{22}) - (\det(\Phi_{12}))^2 = 0. \quad (10)$$

The normalized value Q_1 is newly defined, therefore, as the index of homogeneity:

$$Q_1 \triangleq \frac{(\det(\Phi_{12}))^2}{\det(\Phi_{11})\det(\Phi_{22})}. \quad (11)$$

In the crack-free case, Q_1 becomes **unity** all over the object surface. On the other hand, when the incident wave is scattered by cracks, Q_1 decreases to **zero**.

NUMERICAL EXPERIMENTS

Discrete Models

The finite-difference time-domain (FDTD) method was first introduced for the study of electromagnetic scattering problems (Yee, 1966). In acoustics, the FDTD method has been developed to study a wide variety of problems (Botteldooren, 1994, 1995). By employing finite differential equations to approximate the derivatives and offsetting the stress and the particle evaluation points, both temporally and spatially, the acoustical wave field in solid can be solved. In the isotropic material, the following differential equations govern the particle motion and momentum (Graff, 1991):

$$\rho \frac{\partial \mathbf{v}}{\partial t} = \nabla \cdot \mathbf{T}, \quad \frac{\partial \mathbf{T}}{\partial t} = \mathbf{C} \nabla_S \mathbf{v}. \quad (12)$$

Here the particle velocity vector is \mathbf{v} , the density ρ , and the stress vector in the material \mathbf{T} that can be defined as:

$$\begin{aligned} \mathbf{T} &= (T_1 \quad T_2 \quad T_3 \quad T_4 \quad T_5 \quad T_6)^T \\ T_1 &= T_{xx}(x, y, z, t), \quad T_2 = T_{yy}(x, y, z, t), \quad T_3 = T_{zz}(x, y, z, t), \\ T_4 &= T_{yz}(x, y, z, t) = T_{zy}(x, y, z, t), \quad T_5 = T_{zx}(x, y, z, t) = T_{xz}(x, y, z, t), \quad T_6 = T_{xy}(x, y, z, t) = T_{yx}(x, y, z, t). \end{aligned} \quad (13)$$

The matrix, \mathbf{C} , denotes the elastic stiffness tensor of isotropic material. And the differential operators in Eq.(12) are defined respectively as:

$$\nabla \cdot = \begin{pmatrix} \frac{\partial}{\partial x} & 0 & 0 & 0 & \frac{\partial}{\partial z} & \frac{\partial}{\partial y} \\ 0 & \frac{\partial}{\partial y} & 0 & \frac{\partial}{\partial z} & 0 & \frac{\partial}{\partial x} \\ 0 & 0 & \frac{\partial}{\partial z} & \frac{\partial}{\partial y} & \frac{\partial}{\partial x} & 0 \end{pmatrix}, \quad \nabla_s = \begin{pmatrix} \frac{\partial}{\partial x} & 0 & 0 \\ 0 & \frac{\partial}{\partial y} & 0 \\ 0 & 0 & \frac{\partial}{\partial z} \\ 0 & \frac{\partial}{\partial z} & \frac{\partial}{\partial y} \\ \frac{\partial}{\partial z} & 0 & \frac{\partial}{\partial x} \\ \frac{\partial}{\partial y} & \frac{\partial}{\partial x} & 0 \end{pmatrix}, \quad (14)$$

The differential equations for the above equations can be approximated as following discrete formulas:

$$\mathbf{v}^{[i,j,k]}(n+1/2) = \mathbf{v}^{[i,j,k]}(n-1/2) + \frac{\Delta t}{\rho} \begin{pmatrix} \frac{T_1^{[i+1,j,k]}(n) - T_1^{[i,j,k]}(n)}{\Delta x} + \frac{T_3^{[i,j,k]}(n) - T_3^{[i,j,k-1]}(n)}{\Delta z} + \frac{T_0^{[i,j,k]}(n) - T_0^{[i,j-1,k]}(n)}{\Delta y} \\ \frac{T_2^{[i,j+1,k]}(n) - T_2^{[i,j,k]}(n)}{\Delta y} + \frac{T_4^{[i,j,k]}(n) - T_4^{[i,j,k-1]}(n)}{\Delta z} + \frac{T_6^{[i,j,k]}(n) - T_6^{[i,j-1,k]}(n)}{\Delta y} \\ \frac{T_5^{[i,j,k+1]}(n) - T_5^{[i,j,k]}(n)}{\Delta z} + \frac{T_7^{[i,j,k]}(n) - T_7^{[i,j-1,k]}(n)}{\Delta y} + \frac{T_8^{[i,j,k]}(n) - T_8^{[i,j-1,k]}(n)}{\Delta x} \end{pmatrix},$$

$$\mathbf{T}^{[i,j,k]}(n+1) = \mathbf{T}^{[i,j,k]}(n) + C \Delta t \begin{pmatrix} \frac{v_x^{[i,j,k]}(n+1/2) - v_x^{[i-1,j,k]}(n+1/2)}{\Delta x} \\ \frac{v_y^{[i,j,k]}(n+1/2) - v_y^{[i,j-1,k]}(n+1/2)}{\Delta y} \\ \frac{v_z^{[i,j,k+1]}(n+1/2) - v_z^{[i,j,k]}(n+1/2)}{\Delta z} \\ \frac{v_x^{[i,j,k+1]}(n+1/2) - v_x^{[i,j,k]}(n+1/2)}{\Delta z} + \frac{v_z^{[i,j+1,k]}(n+1/2) - v_z^{[i,j,k]}(n+1/2)}{\Delta y} \\ \frac{v_y^{[i,j,k+1]}(n+1/2) - v_y^{[i,j,k]}(n+1/2)}{\Delta z} + \frac{v_z^{[i+1,j,k]}(n+1/2) - v_z^{[i,j,k]}(n+1/2)}{\Delta x} \\ \frac{v_x^{[i,j+1,k]}(n+1/2) - v_x^{[i,j,k]}(n+1/2)}{\Delta y} + \frac{v_z^{[i+1,j,k]}(n+1/2) - v_z^{[i,j,k]}(n+1/2)}{\Delta x} \end{pmatrix}. \quad (15)$$

Here Δx , Δy , Δz , and Δt are the spatial and temporal step sizes, respectively. The superscript indicates the spatial location, and the argument indicates the time step. For brevity, the spatial offset between the stress and velocity nodes is suppressed in the index of the discrete forms. Geometry of nodes for stress and particle velocity is shown in Fig.1.

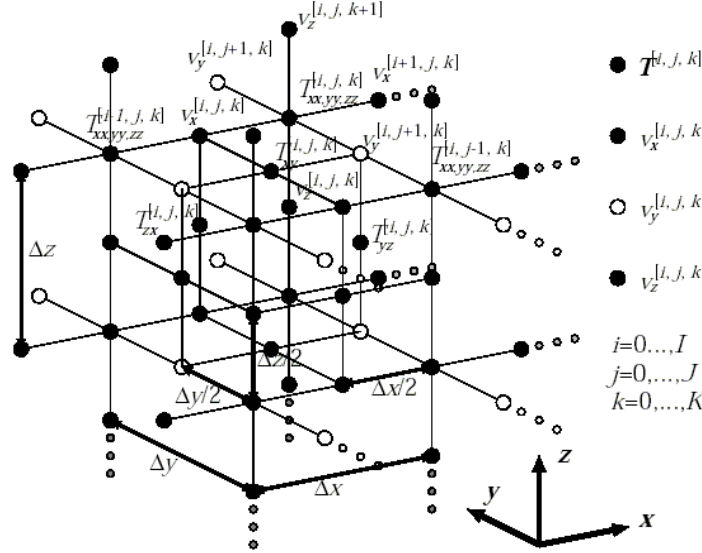


Fig. 1 Geometry of nodes for stress and particle velocity adopted in FDTD simulation.

Consider a three-dimensional computational domain, in which the tapping source is a velocity node at the center of the object surface. Being assumed to be stress-free boundary except the source node, $(I/2, J/2, 0)$. The all surfaces of the object satisfy the stress-free boundary conditions respectively for all $n > 0$. The all values of the stress and particle velocity is initialized to be zero except the source node. In the numerical experiments, the material is considered to be carbon steel as shown in Table 1 (Kino, 1988).

Table 1 Parameters of Simulated Object (carbon steel)

		Size		sampling interval	
Mass density ρ	7.84[10 ³ kg/m ³]	Length	64.0[mm]	Δx	0.25[mm]
Elastic modulus C_{11}	277[GPa]	Width	64.0[mm]	Δy	0.25[mm]
C_{12}	111[GPa]	Height	2.0[mm]	Δz	0.25[mm]
C_{44}	82.9[GPa]			Δt	1.0[ns]

The plot of particle velocity at the source node and the geometry of specimen are shown in Fig.2 (a) and (b) respectively. Fig.3 (a) and (b) show the vertical component of the particle velocity on the object surface. The corresponding indices of surface homogeneity are plotted in (c) and (d) respectively. The major wave fronts yield the phase velocity to be 460m/s, which corresponds to the first anti-symmetric mode, A_0 , of *Lamb* wave velocity. The index of homogeneity increases to unity, because the linear dependency is maintained almost all over the surface.

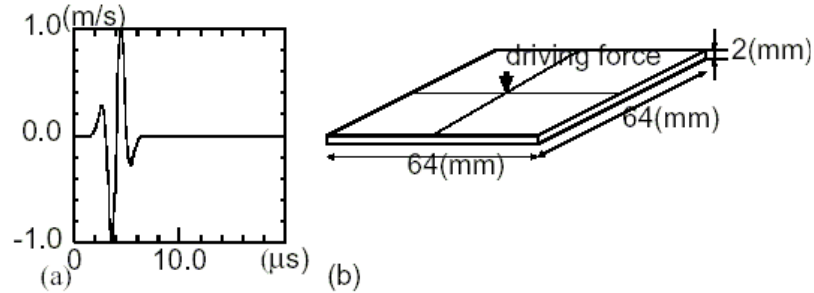


Fig. 2 (a) Particle speed at the source node, (b) geometry of the specimen

Reflection by Crack

Numerical experiments are conducted to assess the performance of the proposed index of homogeneity. A crack considered in this study is illustrated in Fig.4 (a) and stress free boundary conditions adjacent to the crack are introduced into the FDTD simulation as shown in (b). The snapshots of the vertical component of the particle velocity and the corresponding index of homogeneity are shown in Fig.5(a)(b) and (c)(d) respectively. The comparison between the corresponding pair of figures clarifies the effectiveness of the index of homogeneity. The bright areas in the index of homogeneity, (c) and (d), arise from the overlaps of the incident wave and the reflected wave by the cracks. As a consequence of the fact, the proposed index can detect the existence of the cracks on the surface.

CONCLUSIONS

This paper proposes an index homogeneity that is independent of frequency and phase velocity and presents simple digital signal processing algorithm that characterizing the wave field where incident and scattered waves overlap each other.

For detecting the cracks, spatio-temporal gradient analysis based on the linear dependency among the vertical displacement, the vertical particle velocity, and a pair of shear strains is used. By analyzing the covariance matrix of the spatio-temporal gradient vector, it is found that the

proposed index of homogeneity becomes unity only when the surface is perfect, without crack or any fault. The numerical experimental results through FDTD method were conducted with following conclusions. The first is to propose the index of homogeneity that aims to detect the existence of cracks; the second is that the reflected wave fronts by cracks are segregated from the rest of the wave field with introducing the index of homogeneity.

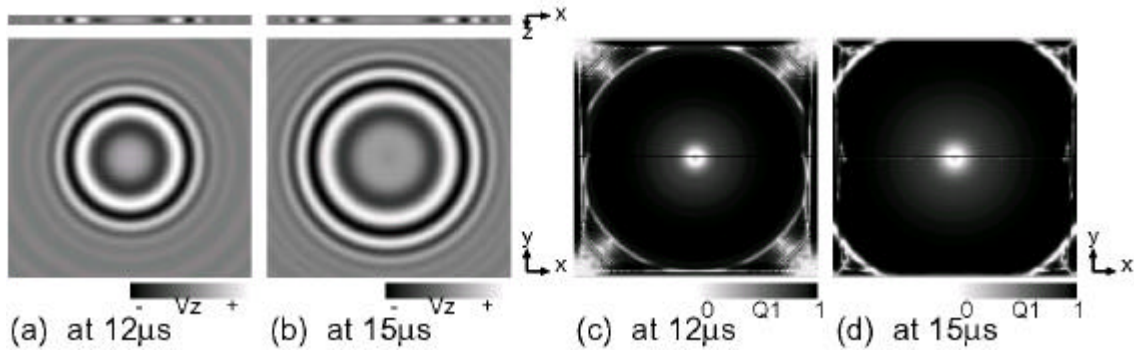


Fig. 3 Vertical particle velocity of the crack-free (perfect) surface: (a)(b), and corresponding index of homogeneity: (c)(d).

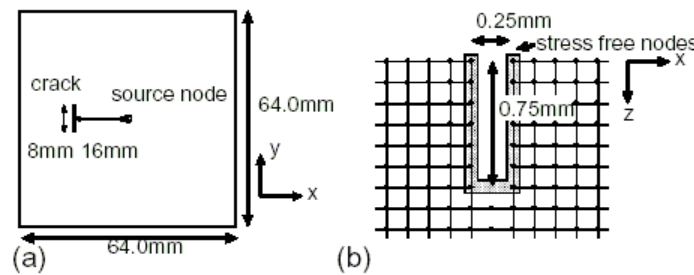


Fig. 4 (a) Cracked specimen, (b) stress-free boundary conditions.

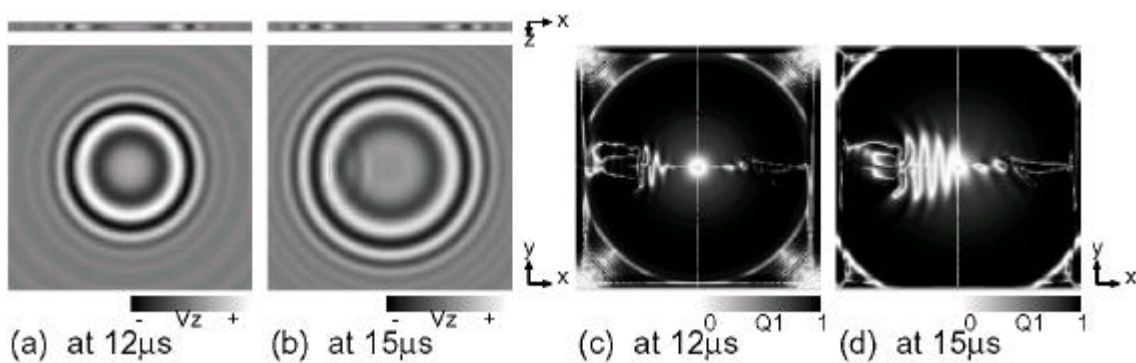


Fig. 5 Vertical particle velocity of the cracked surface: (a)(b), and corresponding index of homogeneity: (c)(d)